Journal Pre-proofs

Research paper

A drug-incorporated-microparticle-eggshell-membrane-scaffold (DIMES) dressing: a novel biomaterial for localised wound regeneration

Rosemond A Mensah, Michael T Cook, Stewart B Kirton, Victoria Hutter, David YS Chau

PII: S0939-6411(23)00179-0
DOI: https://doi.org/10.1016/j.ejpb.2023.07.007
Reference: EJPB 14061

To appear in: *European Journal of Pharmaceutics and Biopharmaceutics*

Received Date: 2 May 2023
Revised Date: 12 July 2023
Accepted Date: 15 July 2023

Please cite this article as: R.A. Mensah, M.T. Cook, S.B. Kirton, V. Hutter, D. YS Chau, A drug-incorporated-microparticle-eggshell-membrane-scaffold (DIMES) dressing: a novel biomaterial for localised wound regeneration, *European Journal of Pharmaceutics and Biopharmaceutics* (2023), doi: https://doi.org/10.1016/j.ejpb.2023.07.007

A drug-incorporated-microparticle-eggshell-membrane-scaffold (DIMES) dressing: a novel biomaterial for localised wound regeneration

Rosemond A Mensah[1,2] , Michael T Cook[1,3], Stewart B Kirton[1], Victoria Hutter[1], David YS Chau[1,2,*]

[1]School of Clinical and Pharmaceutical Sciences, University of Hertfordshire, Hatfield, UK

[2]Eastman Dental Institute, University College London, London, UK

[3]School of Pharmacy, University College London, London, UK

*Corresponding author: d.chau@ucl.ac.uk

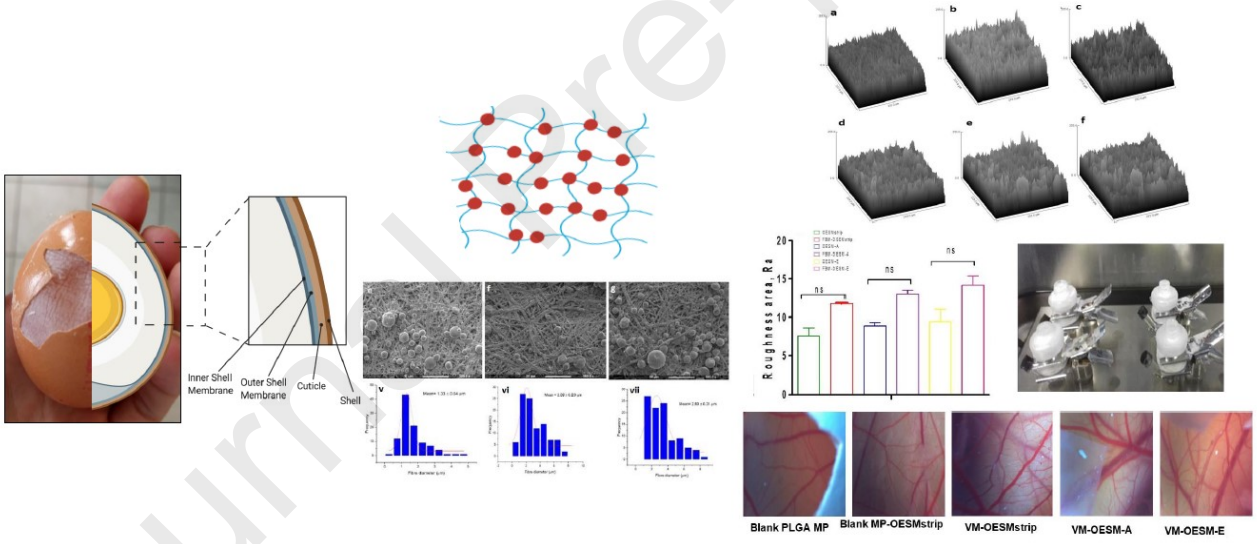

Eggshell membrane (ESM)

Incorporation of drug-loaded microparticles

Material characterisation and drug release/functionality assessment

KEYWORDS

Scaffold, tissue engineering, collagen, drug-release, skin, biomaterials, cell culture, pharmaceutics

ABSTRACT

Chronic wounds affect millions of people annually and have emotional and financial Implications in addition to health issues. The current treatment for chronic wounds involves the repeated use of bandages and drugs such as antibiotics over an extended period. A cost-effective and convenient solution for wound healing is the development of drug-incorporated bandages. This study aimed to develop a biocompatible bandage made of drug-incorporated poly (lactic-co-glycolic acid) (PLGA) microparticles (MPs) and eggshell membrane (ESM) for cornea wound healing. ESM has desirable properties for wound healing and can be isolated from eggshells using acetic acid or ethylenediaminetetraacetic acid (EDTA) protocols. Fluorescein isothiocyanate-labelled Bovine Serum Albumin (FITC-BSA) was used as a model drug, and the PLGA MPs were fabricated using a solvent extraction method. The MPs were successfully attached to the fibrous layer of the ESM using NaOH. The surface features of the ESM samples containing MPs were studied using a field emission scanning electron microscope (FESEM) and compared with blank ESM images. The findings indicated that the MPs were attached to the ESM fibres and had similar shapes and sizes as the control MPs. The fibre diameters of the MPs samples were assessed using Fiji-ImageJ software, and no significant changes were observed compared to the blank ESM. The surface roughness, Ra values, of the MPs incorporated ESM samples were evaluated and compared to the blank ESM, and no significant changes were found. Fourier transform infrared (FTIR) spectroscopy was used to analyse the chemical Composition of the bandage, and the spectra showed that the FBM were effectively incorporated into the ESM. The FTIR spectra identified the major peaks of the natural ESM and the PLGA polymer in the bandage. The bandage was transparent but had a reduced visibility in the waterproof test card method. The bandage achieved sustained drug release up to 10 days and was found to be biocompatible and non-toxic in a chorioallantoic membrane (CAM) assay. Overall, the drug-incorporated PLGA MPs-ESM bandage has great potential for treating chronic wounds.

1. INTRODUCTION

Current approaches to accelerate wound closure and aid the healing process for both dermal and ophthalmological ailments include bandages and topically administered drugs (1-3). However, these methods have limitations such as poor bioavailability, the need for repeated application, and poor patient compliance. To overcome these shortfalls, technologies and protocols exploring the use of controlled drug delivery systems such as hydrogels, nanoparticles, microparticles, implants, dendrimers, microneedles, mucoadhesive polymers, and iontophoresis have been considered (4-8). In essence, these approaches aim to improve the bioavailability and therapeutic efficiency of pharmaceutical formulations, with minimal toxicity, side effects as well as ensuring patient compliance and easing the logistical manipulation by the end-user (4-6,9). Microparticles, in particular, have shown promising results for both skin and ocular drug delivery in various studies as well as optimal characteristics for formulation development (5-6).

Skin and cornea wound healing are similar as both involve a complex sequence of cellular and molecular events aimed at repairing and regenerating damaged tissue. In both cases, the wound healing process can be divided into three overlapping phases: inflammation, proliferation, and remodelling (1, 10-12). During the inflammation phase, immune cells are recruited to the site of injury to remove debris and prevent infection. In the proliferation phase, new blood vessels and connective tissue are formed, and cells such as fibroblasts and keratinocytes proliferate to fill in the wound bed. Finally, during the remodelling phase, the tissue is remodelled and strengthened to restore its original structure and function (1, 10-15). In addition to these broad similarities, there are also some specific similarities between skin and cornea wound healing. For example, both skin and cornea have an outer layer that serves as a barrier to the external environment, and both have specialized cells such as keratinocytes and epithelial cells that play important roles in the healing process. Furthermore, both skin and cornea are exposed to environmental stresses that can interfere with wound healing, such as ultraviolet (UV) radiation and microbial infection. Finally, both skin and cornea wounds can result in scarring, which can have functional and cosmetic consequences (1-2, 11-14).

In a simplistic overview, the optimal wound healing process requires a moist and permeabilised environment to ensure the correct cellular processes and matrix deposition required. An ideal biomaterial for chronic wound bandages should be biocompatible, non-toxic, transparent, comfortable for the patient, and easy to apply (16). Researchers are exploring the use of various biomaterials, including natural and synthetic polymers, to develop effective bandages: the more advanced/enhanced versions being "smart"- being able to respond to the rapidly changing microenvironment, deliver therapeutic agents, and favourable to the end-user. As such, number of candidate materials have been investigated which include animal/non-animal derivatives, drug incorporated therapeutic dressings, hydrocolloids and semi-permeable hydro-films (17-20). Moreover, advancements in nanotechnology, stem cell research, and gene therapy may provide new opportunities to enhance corneal wound healing and reduce the need for corneal transplantation (21-22).

The eggshell membrane (ESM) is a naturally occurring sustainable materially formed from bio-polymeric fibres that is gaining attention for its potential biomedical applications. It has a unique structure and is readily available as a resource (23-27). The ESM is the clear film lining the eggshell and consists of two distinguishable sides: the inner side, also known as the limiting membrane (LM),

is non-fibrous and smooth, while the outer side is made up of two layers, the inner shell membrane (IM) and the outer shell membrane (OM), which is firmly attached to the eggshell (23, 27). The outer shell membrane can only be detached by dissolving the calcium carbonate in the eggshell (23).

The ESM contains various biochemical components such as collagen, hyaluronic acid, glucosamine, glycosaminoglycans, and fibronectin, which are responsible for its biological, physical, and mechanical properties (22-26, 29-33). Proteome analysis by Ahmed *et al*., (26) identified a total of 251 different proteins in ESM, giving a huge diversity of chemical structure on the membrane. There are three different methods of separating ESM from the eggshell: manual peeling, chemical treatment, and mechanical extraction (23-24,27, 34-39). The mode of application of ESM is dependent on the extraction method. Manual peeling and chemical treatment generate an intact membrane, while the mechanical method produces fragments of the membrane (24-26). However, these separation methods have some limitations associated with them, such as effects on physical and chemical characteristics, long chemical reaction time, and long separation period (23,26 and 30).

The ESM exhibits high surface area, semi-permeability, and porosity together with its non-toxic nature, biodegradability, anti-inflammatory, and anti-bacterial properties (23,29 and 33). All these unique properties make ESM a valuable biomaterial for various applications, including skin wound healing and regeneration, bone, nerve, and cartilage applications. Furthermore, ESM has the potential to be used as a drug delivery device for drugs or nanoparticles (25, 27-31 and 40). Recently, Araujo and colleagues (41) analysed the use of ESM as a biopolymer in drug delivery studies. The results showed that nimesulide, a hydrophobic drug, was incorporated into the ESM, and although the drug loading results were not promising, the ESM was confirmed to be a potential biomaterial for pharmaceutical formulations due to its biocompatibility and biodegradability. Li *et al*. (40) and Briggs *et al*, (25) have reported bandages consisting of silver nanoparticles (AgNP) and ESM for skin wound care. The results indicated that AgNP was successfully deposited on the ESM, was non-toxic, and had suitable surface area, pore size, and release profile. The aim of this study is to take this promising material formulate and evaluate a potential novel bandage comprising of drug incorporated poly(lactic-co-glycolic acid) (PLGA) MPs and ESM for chronic wound healing applications (Figure 1) herein, and after, referred to as “DIMES”.

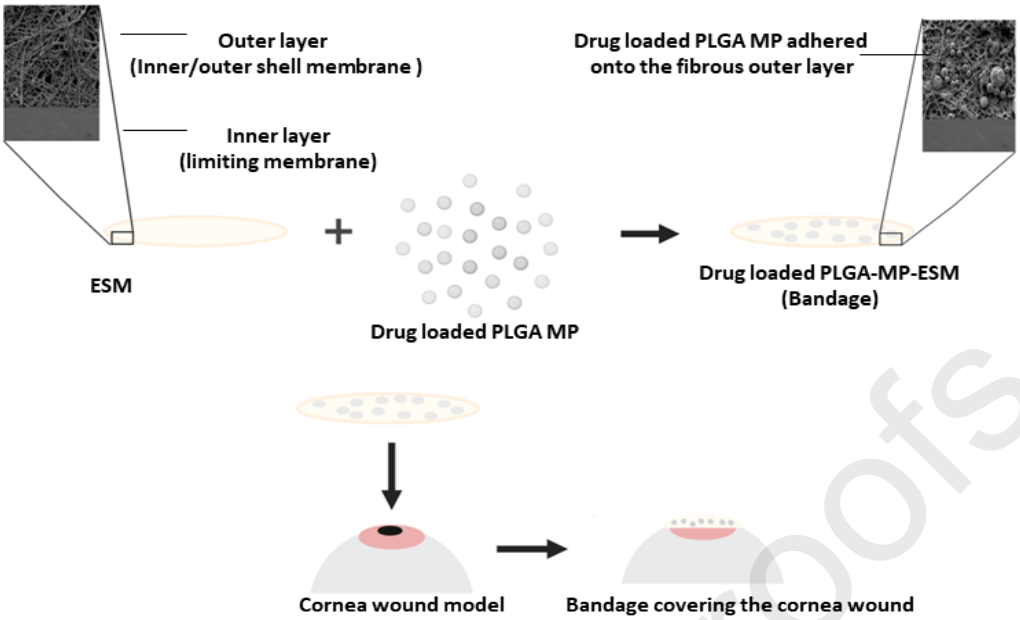

Figure 1. Schematic representation of DIMES fabrication. A summary of the proposed biomedical bandage development to generate the novel wound healing dressing consisting of drug incorporated PLGA microparticles and eggshell membrane. MP–microparticles, ESM-eggshell membrane and PLGA-Poly lactic-co-glycolic acid. Model drug: Fluorescein isothiocyanate-labeled Bovine Serum Albumin (FITC-BSA)

2. MATERIALS AND METHODS

2.1 Materials

PLGA copolymers with lactic: glycolic acid ratios of 1:1 (MW: 29-38 kDa) were purchased from Evonik (Darmstadt, Germany). 99+ % hydrolysed poly (vinyl alcohol) (PVA) (MW: 89-98 kDa), PBS, FITC-BSA, QuantiPro Bicinchoninic Assay (BCA) kit and VEGF were obtained from Sigma-Aldrich (Poole, Dorset, UK). Ethyl acetate (≥ 99.5 %) and acetic acid (≥ 99%) were purchased from Fisher Scientific (Loughborough, Leicester, UK). Free-range brown chicken eggs (British Blacktail) were purchased from a local supermarket (Waitrose, London, UK). Fertilized hens' eggs were purchased from Henry Stewart and Co Ltd (Norfolk, UK). Ethylenediaminetetraacetic acid (EDTA) was supplied by Agar Scientific (Stansted, Essex, UK). The Visking Dialysis Tubing membrane, a regenerated cellulose membrane (MW:12-14 kDa, dry thickness: 20 µm) was purchased from Medicell membrane Ltd (Greenwich, London, UK). All other reagents and chemicals were obtained from Merck (Poole, Dorset, UK) unless otherwise stated. Fresh porcine eyes were kindly donated by the Royal Veterinary Collage (Hertfordshire, Hatfield, UK).

2.2 Methods

2.2.1 Preparation of drug-incorporated microparticle ESM

Fresh eggs were carefully washed in deionised water before being submerged in 0.5 M acetic acid for 44 h (ESM-A) or 0.9 M EDTA for 20 h at room temperature (19 °C) (ESM-E). The extracted membranes were collected and extensively washed in DI water to remove the albumen and yolk after the calcium carbonate shell had completely dissolved (40). The ESM was manually removed from the eggshell using tweezers as a control (ESMstrip). To avoid dehydration, all extracted ESM samples were fully immersed in PBS and stored in a refrigerator (4 °C) before use. The drug incorporated was generated using the in-house method developed (Mensah *et al*, 23). Briefly, 20 mg FITC-BSA (model drug) or 20 µg VEGF was dissolved in 5 ml of ethyl acetate in which 1 g of PLGA polymer was completely pre-dissolved. A primary emulsion of FITC-BSA/PLGA/EAc or VEGF/PLGA/EAc and PVA solutions were formed and vortexed to create the MPs. Following that, the emulsion was added to a hardening bath to allow for complete evaporation (24h). The hardening bath was completely covered with aluminium foil to exclude light. The supernatant was collected before the formulated MPs were filtered, washed, and freeze-dried.

The loading capacity (LC%) and the encapsulation efficiency of the generated MPs were examined by an indirect technique that involved the use of the Micro-QuantiPro™ BCA Assay Kit (Sigma-Aldrich, Poole, Dorset, UK) to determine the amount of FITC-BSA or VEGF present in the supernatant collected after the filtration and washing of the formulated MPs. To ascertain the amount of FITC-BSA or VEGF that was encapsulated, a mass balance calculation was executed. The EE% and LC% were calculated using Equation (1) and (2) respectively below:

$$LC\% = \frac{amount\ of\ protein\ entrapped}{total\ microparticle\ weight}$$

(Equation 1)

$$EE\% = \frac{total\ protein\ added - free\ unentrapped\ protein}{total\ drug\ added}$$

(Equation 2)

Prior to loading the drug incorporated microparticles to the outer layers of the ESMs (OESM), a preliminary structural study was performed using both the OESM and inner layer of the ESM (IESM). The outer layers were identified as the ideal layer to load the MPs. To prepare the FITC-BSA incorporated MPs (FBM), or VEGF incorporated MPs (VM) OESMs, 50 mg of the generated MPs were immersed in 1 ml of aqueous 0.2 M NaOH, alkaline-catalyzed hydrolysis for 30 seconds (modified method adapted from Amoyav and Ofra, (42), Figure 2A). The modified MPs were washed three times with dH_20 (i.e. three cycles of centrifugation at 3000rpm for 2min per solvent change) to remove the NaOH residue. The MPs were incorporated onto the outer layer (fibrous side) of 3 x 3 cm^2 membranes. Using a spatula, the MPs were spread on the outer layer of the ESM samples (Figure 2B). The generated FBM incorporated OESMs samples (FBM-OESMstrip, FBM-OESM-A and FBM-OESM-E) and VM incorporated OESMs samples (VM-OESMstrip, VM-OESM-A and VM-OESM-E) were washed to remove excess MPs, freeze-dried at room temperature (19 °C) and stored at 4 °C for characterisation. The residue from the washing process was filtered, and the MPs collected were air-dried and weighed to determine the quantity of MPs incorporated on the ESMs.

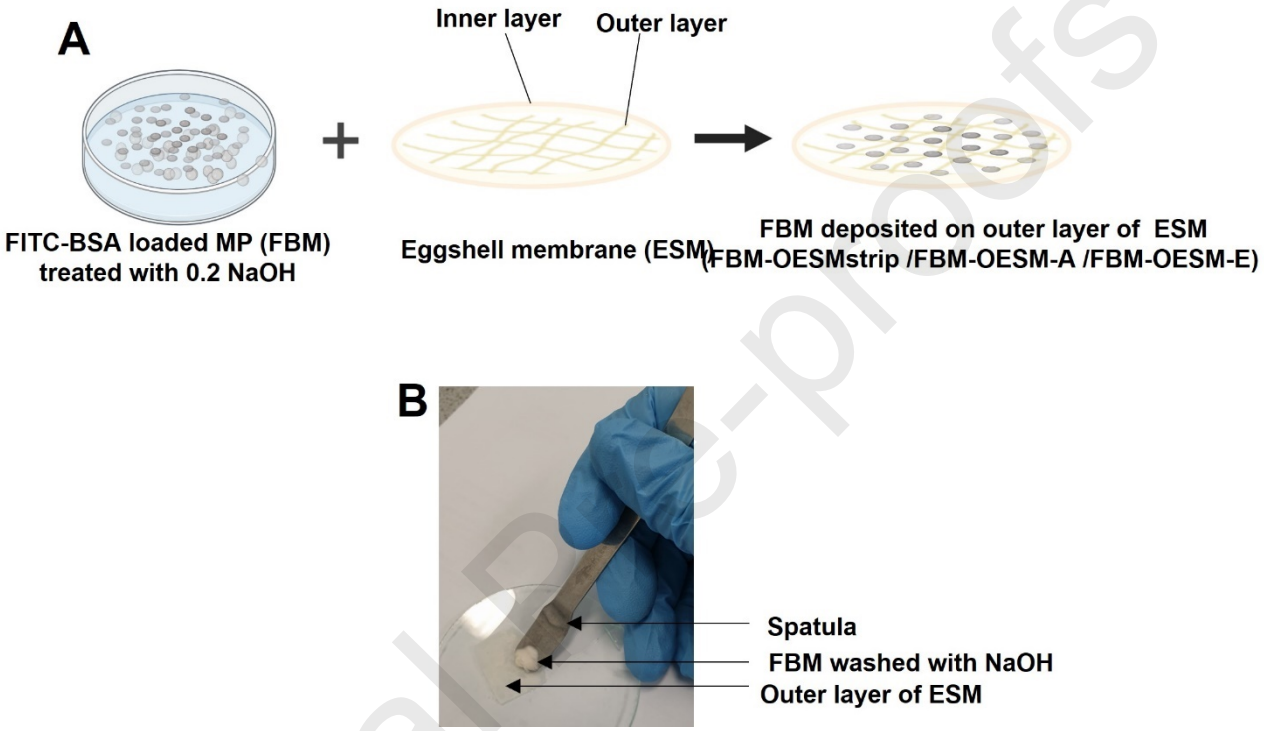

Figure 2 (A) Schematic diagram of the fabrication of DIMES using the chemical treatment method: alkaline-catalysed hydrolysis. They were immersed in 0.2 M NaOH for 30 minutes, the MPs were washed three times to remove excess NaOH. The modified MP were then spread on the ESM, washed, air- dried at room temperature (19 °C) and stored at 4 °C. The microparticles were incorporated onto the outer layer (fibrous side) of the membranes. (B) Photograph of the preparation of the drug incorporated microparticles ESM. The microparticles were washed with NaOH before spreading on the membrane. OESM represents the outer layer of eggshell membrane, FITC-BSA represents Fluorescein isothiocyanate-labeled bovine serum albumin and MP represents microparticles.

2.2.2. Characterisation

2.2.2.1. Surface Morphology. Freshly made FBM-OESMstrip, FBM-OESM-A and FBM-OESM-E were fixed for 24 hours at 4 °C in 3 % (w/v) glutaraldehyde in 0.1 M cacodylate buffer. The fixed membranes were then dehydrated for 2 minutes in a series of graded ethanol solutions (v/v): 1 x 70%, 1 x 90%, and 3 x 100%. The membranes were then subjected to critical point drying by immersing them in

hexamethyldisilane (HMDS) for 2 minutes. The dried membranes were adhered to 12 mm carbon tabs (Agar Scientific, Stansted, UK) that were pre-mounted onto 0.5 mm aluminium spectrum stubs (Agar Scientific, UK) before being sputter-coated with gold/palladium (Polaron E500, Quorum Technology, UK). The morphological characteristics of the FITC-BSA MPs, VEGF MPs and the FITC-BSA MPs incorporated ESMs were measured using Philips XL30 FESEM (UK) at an operating voltage of 5 kV, spot size 3. The samples were examined at a magnification of 500x. The particle size distributions of the FITC-BSA MPs and VEGF MPs, and fibre diameters of the blank OESMs and FITC-BSA MPs incorporated OESMs in the FESEM images were evaluated via Fiji-ImageJ software and OriginLab Origin 2021. Using the FESEM images at Magnification of 500x generated for OESMstrip, OESM-A and OESM-E, FBM-OESMstrip, FBM-OESM-A and FBM-OESM-E, the surface roughness was examined. Surface topography and surface roughness plots were generated using Fiji-ImageJ software. Based on the surface topography and profile plots, the surface roughness (Arithmetical mean deviation, Ra) was deduced via SurfCharJ-1q plugin in the Fiji-ImageJ software.

2.2.2.2. Transparency tests. To determine the transparency qualities of FBM-OESMstrip, FBM-OESM-A and FBM-OESM-E, the samples were soaked in PBS for 24 hours to equilibrate, and the wet samples were placed over a standardised waterproof test card. The images of the samples were taken with a Samsung Galaxy S9 plus 12 MPS Super Speed Dual Pixel AF sensor camera (OIS, FOV: 77, Dual Aperture: F1.5 mode/ F2.4 mode) (Chau *et al*,39; Mensah *et al*, 19). Further transparency of the samples was examined by measuring light transmittance through wet samples with a T80 UV-VIS spectrophotometer (PG instrument Ltd., Leicester, UK) over a wavelength range of 400 to 1000 nm (method adapted from Mensah *et al*, 23).

2.2.2.3. Fourier-transform infrared spectroscopy. A PerkinElmer FTIR operating in the Attenuated Total Reflectance mode (SensIR Technologies, UK) was used to determine the elements and functional groups of the FBM-OESMstrip, FBM-OESM-A and FBM-OESM-E. The samples were scanned in the infrared range 600–4000 cm^{-1} and measured at 19 °C. Before analysing the samples, the spectrometer was calibrated by taking a background spectrum.

2.2.2.4. Porosity. A previously reported liquid displacement method was employed to determine the porosity of the FBM-OESMstrip, FBM-OESM-A and FBM-OESM-E (19, 41). In brief, the samples were air dried for 24 hours at room temperature (~19 °C) and weighed. The dried samples were then immersed in 5 ml of PBS for 24 hours at 34 °C before being weighed after patting the surfaces with a paper towel. The total pore volume was calculated using the average thickness (mm) and diameter of the FBM-incorporated ESM samples (Equation 3). The porosity was calculated as shown in Equation 4 below (n=3).

$$V_{\circ} = (\square \times \frac{D}{2})^{2} x H$$ Equation 3

$$\mathcal{E}\,(\%)\frac{W_w\,x\,W_d}{\rho\,x\,V_\circ}x\,100 \qquad \text{Equation 4}$$

Where, V_o is the total pore volume, D is the diameter, H is the thickness, Ww and Wd are the wet and dry weights of the samples, ε is the porosity and ρ is the density of PBS. The thickness of the FBM-incorporated OESMs and blank MP OESMs were measured by sandwiching them between two known-thickness microscopic slides. The total thickness of the samples was measured to the nearest 0.01 mm using a Moore and Wright Outside micrometre (Zoro, Leicester, UK). Each sample's thickness was measured at six random locations, and the average values were reported as the membrane thickness (40).

2.2.2.5. Wettability. The contact angle of a PBS solution droplet (~2.0 µL) was measured using an optical contact angle meter (200 CAM, KSV Instruments Ltd, Finland) to assess the surface wettability of FBM-OESMstrip, FBM-OESM-A and FBM-OESM-E at room temperature (~19 °C). using the static sessile drop method as previously described Mensah *et al*., (23). In short, a small droplet of PBS solution (~2.0 µL) was deposited on the horizontal membrane surface and a side view phot was taken using 200 CAM optical contact angle meter (KSV Instruments Ltd, Finland) at room temperature (~19° C) to measure the contact angle at 10 seconds (Figure S1). Each value of the contact angle was calculated as an average of three different readings taken under the same conditions.

***2.2.2.6. In vitro* release study with diffusion cell.** The drug release profile of the fabricated MPS-ESMs was examined using an *in vitro* Franz diffusion cell eye model generated by Shafaie *et al*, (45). The bespoke Franz cell used consisted of three compartments: a donor chamber, a middle chamber containing porcine vitreous humour and a receptor chamber (Figure S2). A small incision was made on the lateral side of the *porcine* eye with a scalpel to extract the vitreous humour. Vitreous humour was gently *separated* onto a petri dish, and non-vitreous parts attached to it, such as the iris and lens, were separated further. Extracted vitreous was stored in sterile containers at 2-8 °C. The isolated vitreous was used within 12 h of the extraction. The middle chamber was filled with vitreous, and the top and bottom were covered with a cellulose dialysis membrane. Subsequently, the donor and receptor chambers were attached. The set up was occluded with parafilm to prevent evaporation. The FBM-OESMstrip, FBM-OESM-A and FBM-OESM-E were trimmed into circular discs of diameter 10 mm sufficient to cover the diffusion area of the donor chamber. Each membrane sample was mounted between the donor chamber and middle chamber with drug incorporated side (outer layer) facing upwards. For the study of free FBM (control), the 30 mg sample was introduced directly onto the cellulose dialysis membrane at the top. Using a syringe, 3 ml of PBS was introduced into the receptor chamber with magnetic stirrer and allowed to equilibrate at 34 °C (natural temperature of the eye) for 30 minutes. Thereafter, 1 ml of the PBS was introduced into the donor chamber. FITC-BSA sample volume of 3 ml were collected though the sampling port of the cell at varying times within 14 days. The FITC-BSA samples were centrifuged and the concentration of the protein in each sample was determined using Micro-QuantiPro™ BCA Assay kit. Each time an equal volume of fresh preheated PBS was reintroduced into the receptor chamber to main sink conditions. The air bubbles formed were removed by carefully tilting the Franz cell for the bubbles to escape through the sampling port. The cumulative percentage released was calculated, and the mean values and standard deviations were reported.

***2.2.2.7. In ovo* chick chorioallantoic membrane (CAM) assay.** The *in ovo* CAM assay was employed, as previously described (46) to determine the toxicity and biocompatibility of the drug incorporated MPS-ESMs (Figure S3). Fertilized Dekalb White chicken eggs (Henry Stewart and Co Ltd, Norfolk, UK) were incubated for four days in a Brinsea Eco incubator at 37 °C and 80 % relative humidity. On the fourth day, 5 ml of egg white was extracted with a blunt 18-gauge needle through a hole to reduce the volume space within the egg and result in a lower/detachment of the CAM from the top portion of the eggshell. In each egg, a 2 x 2 cm square window opening was cut and covered with transparent low adhesion tape. The eggs were incubated for an extra day. Blank MP-OESMstrip, blank MP-OESM-A, blank MP-OESM-E, VM-OESMstrip, VM-OESM-A and VM-OESM-E samples immersed in PBS were sterilised under UV irradiation in laminar cell culture for 24 hours- a process that had been optimized previously and demonstrated no changes to the stability or chemical composition of the drug-incorporated MPs (46-47). On the 5th day, the pre- sterilised samples were placed on the CAM. The sides without the MPS were placed directly on the CAM. Additionally, 3 x 3 mm Whatman #1 filter paper squares, blank MPS, VEGF incorporated MPs and VEGF were sterilized using 70% ethanol. The filter papers socked with VEGF incorporated MPs 20 L were placed on the CAM. Using a 100 mm micro spatula, 20 µg of blank MPs, 20 µg of VEGF incorporated MPs and 2 µg of VEGF were carefully incorporated on the filter papers previously placed on the CAM. All samples were placed on the CAM under sterile conditions. The windows of the eggs were sealed and kept in the incubator for an additional 5 days and monitored daily. The seal was removed on the tenth day, and photographs were obtained using a GX CAM digital camera at X1 magnification. The AngioQaunt programme (MATLAB, UK) was used to quantify, analyse, and characterise blood vessels (47). The counting of the various vessels in each CAM was random and triplicated.

2.2.3. Statistical analysis

Data are shown as mean ± SD (standard deviation) and compared using 1-way and 2-way ANOVA with Tukey's, Dunnett's or Bonferroni Multiple Comparison Test. Statistical significance is indicated with (*) which represents a $p < 0.05$, (**) which represents a $p < 0.01$, and (***) which represents a $p < 0.001$. No statistical significance is indicated by $p > 0.05$. GraphPad software 9.0, Fiji-ImageJ and OriginLab Origin 2021 software were utilised in analysing the data.

3. RESULTS

3.1. Drug-Incorporated Microparticles eggshell membrane (DIMES)

Using the optimised single o/w emulsion method, 10 – 50 µm MPs were formulated with or without model drugs: FITC-BSA and VEGF. The loading capacity (LC%) and encapsulation efficiency (EE%) of FITC-BSA incorporated in MPs were determined to be 59.03 ± 0.67 and 17.24 ± 0.32, respectively. The LC% and EE% of VEGF incorporated in MPs were found to be 52.42 ± 1.13 and 14.17 ± 1.04, respectively. The ESMs were extracted using manual peeling, immersion in 0.5M acetic acid and immersion in 0.9 M EDTA methods. Drug incorporated microparticles ESMs were generated using chemical treatment method. The water obtained from the washing process was filtered and the MPs collected was air-dried and weighed to determine the total FITC-BSA MPs incorporated (results

summarised in Table 1). The results revealed that more than 60% of the MPs were successfully attached to the outer layer of OESMstrip, OESM-A, OESM-E.

Table 1. Percentage incorporated modified MP in FBM-OESMstrip, FBM-OESM-A and FBM-OESM-E. samples. OESM represents the outer layer of eggshell membrane and FBM represents Fluorescein isothiocyanate-labeled Bovine incorporated microparticles.

Sample	Percentage of incorporated MP (%)
FBM MP-OESMstrip	66.22 ± 1.51
FBM MP-OESM-A	62.56 ± 0.98
FBM MP-OESM-E	67.39 ± 1.65

3.2. Surface Morphological analysis of drug incorporated MPS-ESM

The morphologies of the blank OESMs (Figure 3A-C) and FITC-BSA incorporated MPs (FBM) (Figure 3D) were analysed and compared to the FITC-BSA MPs sample s generated (Figure 3E-G). The images showed the presence of MPs adhered to the nanofibers in the ESM (Figure 3E-G). The MPs attached to the fibres in the ESM have similar spherical-like shapes as the MPs before attachment (Figure 3D). Subsequently, the particle size of the MPs and fibre diameters of the blank OESMs and FITC-BSA MPs incorporated OESMs were evaluated via Fiji-ImageJ software and their respective distribution plots (Figure 3i-vii) were generated with OriginLab Origin 2021. The fibre diameters of OESMstrip, OESM-A and OESM-E were deduced as 0.25 to 5 .75 µm, 0.936 to 8.97 µm and 1.02 to 8.88 µm respectively. From the data (Figure 3iv), FITC-BSA MPs with particles size ranging from 2.56 to 57.5 µm (mean particle size of 17.09 ± 0.25 µm) were incorporated into the ESMs. The fibre diameters of the FBM-OESMstrip, FBM-OESM-A and FBM-OESM-E were evaluated as 0.28-4.75 µm, 0.84 – 8.97 µm and 1.26 – 6.87 µm respectively (Figure 3v, vi and vii). The fibre diameters of the MPs incorporated ESM were assessed and compared to the fibre diameters of blank ESMs. Figure 3viii displays the mean fibre diameter of the drug incorporated ESM and blank ESMs. From the results, no significance changes were observed in the MPs incorporated ESM (i.e., FBM-OESMstrip, FBM-OESM-A and FBM-OESM-E) compared to their respective blank ESM, $p>0.05$ (i.e., OESMstrip, OESM-A and OESM-E). This suggests that the introduction of the MPs did not alter the fibrous structures.

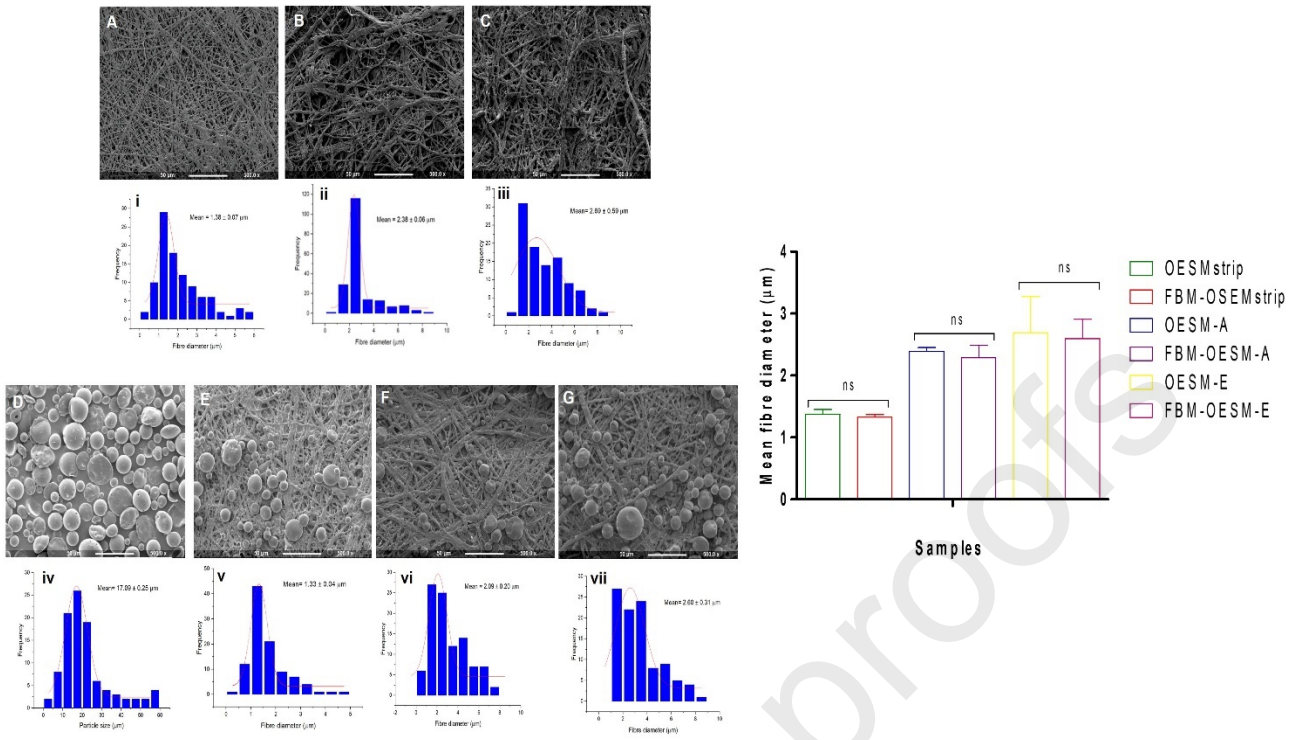

Figure 3. Structural analysis of the fibrous network of the Outer layer of Eggshell membrane (A-C) represents the FESEM images of OESMstrip OESM-A and OESM-E respectively. Structural analysis of FITC-BSA incorporated Microparticles showing FESEM images at 500x magnification of the FITC-BSA incorporated Microparticles (FBM)(D) and the FBM incorporated ESM (G-F) i.e., FBM-OESMstrip, FBM-OESM-A and FBM-OESM-E0. 'i-iii' presents the fibre diameter of OESMstrip, OESM-A and OESM-E respectively. 'iv' represents the particle size distribution plot for the FBM. 'v, vi, vii' represent the fibre diameter distribution (n= 100 counts) for OESMstrip, OESM-A and OESM-E respectively. All values are expressed as mean ± σ for n=100. FBM: FITC-BSA incorporated microparticles. 'viii' represents the Mean fibre diameter of FITC-BSA incorporated Microparticles. The graph shows the results for the comparison of the mean fibre diameter of the OESMstrip to OESM-A and OESM-E to FBM-OESMstrip, FBM-OESM-A and FBM-OESM-E. No significance differences were observed (ns, $p>0.05$). All values are expressed as mean ± SD for n=100 (1-way ANOVA with Bonferroni's multiple comparison post-test ($p>0.05$). FBM: FITC-BSA incorporated microparticles.

The surface roughness of the FITC-BSA MPs incorporated ESM samples were evaluated using the FESEM images at magnification of 500x. Figure 4 represent the surface topography of OESMstrip, OESM-A, OESM-E, FBM-OESMstrip, FBM-OESM-A and FBM-OESM-E, respectively. The images were generated for the surface area of 229 x 330 μm^2 via Fiji-ImageJ software. The surface consists of pine-like surface identical to that of the blank outer layer ESM: OESMstrip, OESM-A and OESM-E. Surface of the MPs incorporated ESM were further characterised by measuring the surface roughness area value i.e., arithmetical mean deviation, Ra. Prior to that, the surface roughness plot was generated via Fiji-ImageJ software. The Ra values obtained for FBM-OESMstrip, FBM-OESM-A and FBM-OESM-E were compared to the corresponding Ra values of the blank ESMs: OESMstrip, OESM-A and OESM-E (Figure 4G). Statistically, no differences were observed between the blank and the MPs incorporated ESMs ($p>0.05$).

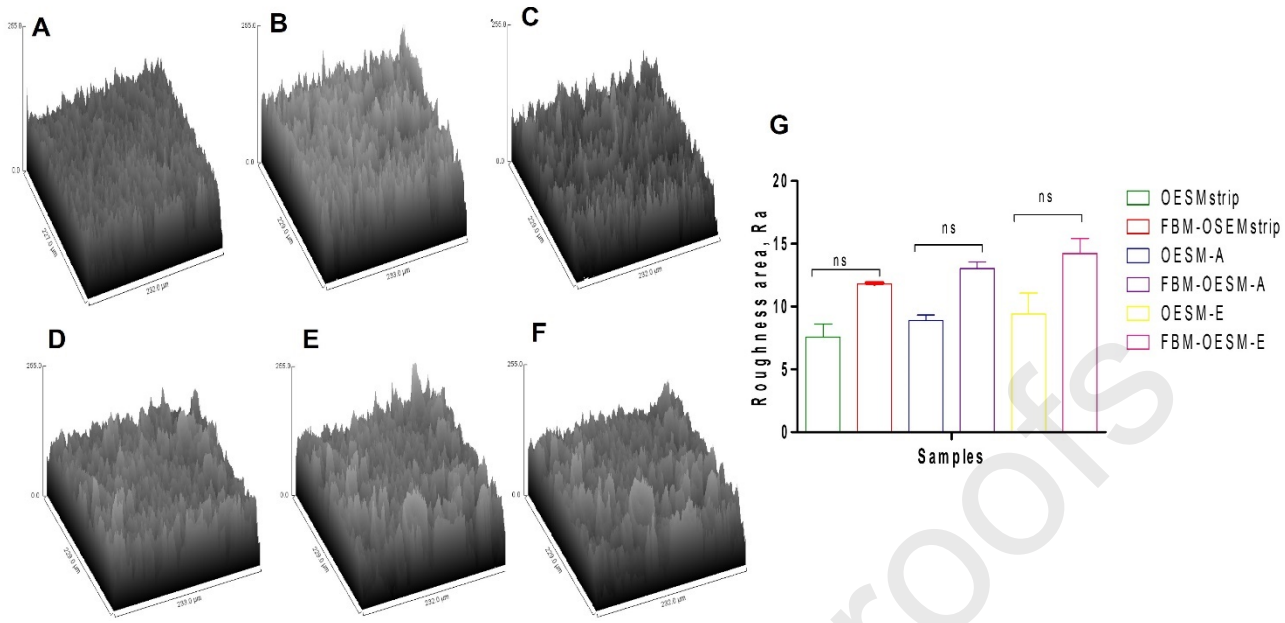

Figure 4. Surface roughness analysis. The images A-F are surface topography of OESMstrip, OESM-A, OESM-E FBM-OESMstrip, FBM-OESM-A and FBM-OESM-E generated via Fiji-ImageJ surface. Image G represents a plot of arithmetical mean deviation, Ra (µm) recorded for outer layers: OESMstrip, OESM-A and OESM-E, and drug incorporated MP ESM: FBM-OESMstrip, FBM-OESM-A and FBM-OESM-E. using FESEM at magnification of 500x on surface area 229.0 X 232.0 µm respectively. The Ra values were calculated via Fiji-ImageJ software SurfCharJ 1q plugin. 1-way ANOVA with Bonferroni's multiple comparison post-test ($p > 0.05$). All values are expressed as mean ± σ for n=10. ns represents no significant difference, $p>0.05$. FBM: FITC-BSA incorporated microparticles.

3.3. Chemical composition

FTIR was employed to characterize the PLGA MPS, the ESMs and the incorporation of the MPS in the ESMs (Figure 5). The PLGA MPS spectrum displayed peaks such as the -CH2, -CH3 stretching vibrations (2946.72 - 3000 cm^{-1}), the carbonyl C=O stretching vibrations of esters (1746.53 cm^{-1}), asymmetrical stretching -CH2, -CH3 (1381.62 cm^{-1} and 1452.06 cm^{-1}) and the C–O stretching vibrations (1180.38 cm-1). The spectrum of blank OESM (Figure 5) displays the presence of peaks (in cm^{-1}) at 3289 (stretching mode of O–H and N–H), 3060, 2932 and 2869 (asymmetric stretching vibrations of the C–H bonds present in =CH and =CH2 groups), 1646 (C=O stretch of amide), 1524 and 1240 (CN stretching/NH bending modes of amide), 1441 (stretching mode of C=C bond), 1066 (stretching mode of C–O bond) and 660 (stretching mode of C–S bond). Figure 5 illustrates that the FTIR spectra of the three ESM samples (FBM-OESMstrip, FBM-OESM-A and FBM-OESM-E) containing the FITC-BSA incorporated microparticles are similar. In the spectra some peaks came from the polymer CH2-CH3 stretching vibrations (2946.72 - 3000 cm^{-1} and 1746.53 cm^{-1}) and these peaks from the ESM :1646 cm^{-1}, 1524 cm^{-1}, 1441 cm^{-1} and 1240 cm^{-1}.

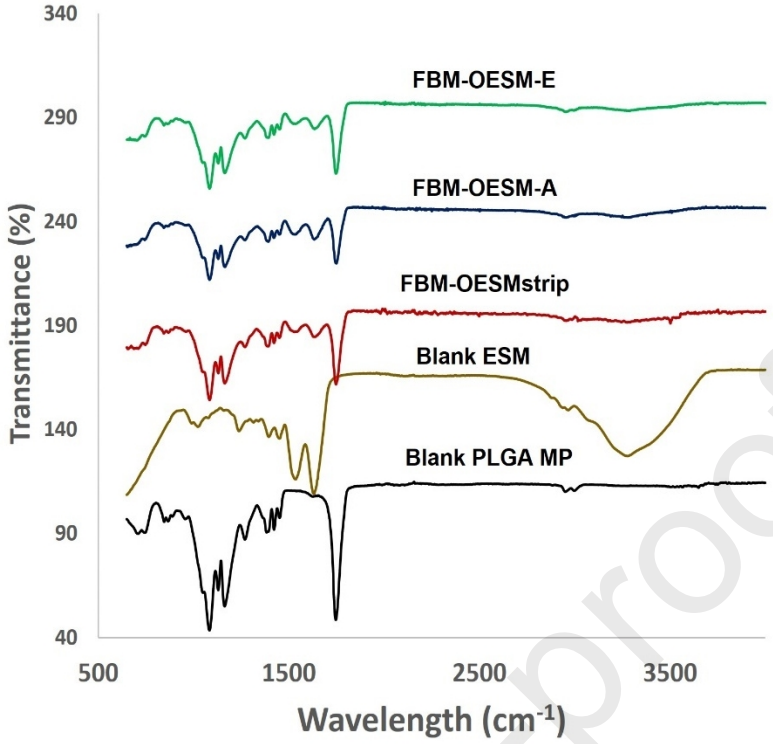

Figure 5. FTIR spectra of FITC-BSA incorporated ESM documenting the FTIR spectra of PLGA MP blank OESM FBM-OESMstrip, FBM-OESM-A and FBM-OESM-E. FBM: FITC-BSA incorporated microparticles.

3.4. Visibility test

The results of the visual observations of the wet blank ESMs and wet drug incorporated MPS ESMs are shown in Figure 6A. The sample test can clearly be seen in the blank ESMs samples: Blank OESMstrip, Blank OESM-A and Blank OESM-E. the visibility of the test in FBM-OESMstrip, FBM-OESM-A and FBM-OESM-E are reduced as compared to the blank ESMs, the MPs incorporated ESM samples are visually transparent. The transparencies of the samples were further characterised by measuring light transmittance using UV-VIS spectrophotometer (Figure 6B). In the results, the observations made in the test card analysis are confirmed. The light transmittance values for FBM-OESMstrip, FBM-OESM-A and FBM-OESM-E are lower than Blank OESMstrip, Blank OESM-A and Blank OESM-E. This suggests that the presence of the MPs in the FBM-OESMstrip, FBM-OESM-A and FBM-OESM-E reduces the visibility. Nonetheless, the light transmittance values for both blank and MPs incorporated ESMs were above 70%.

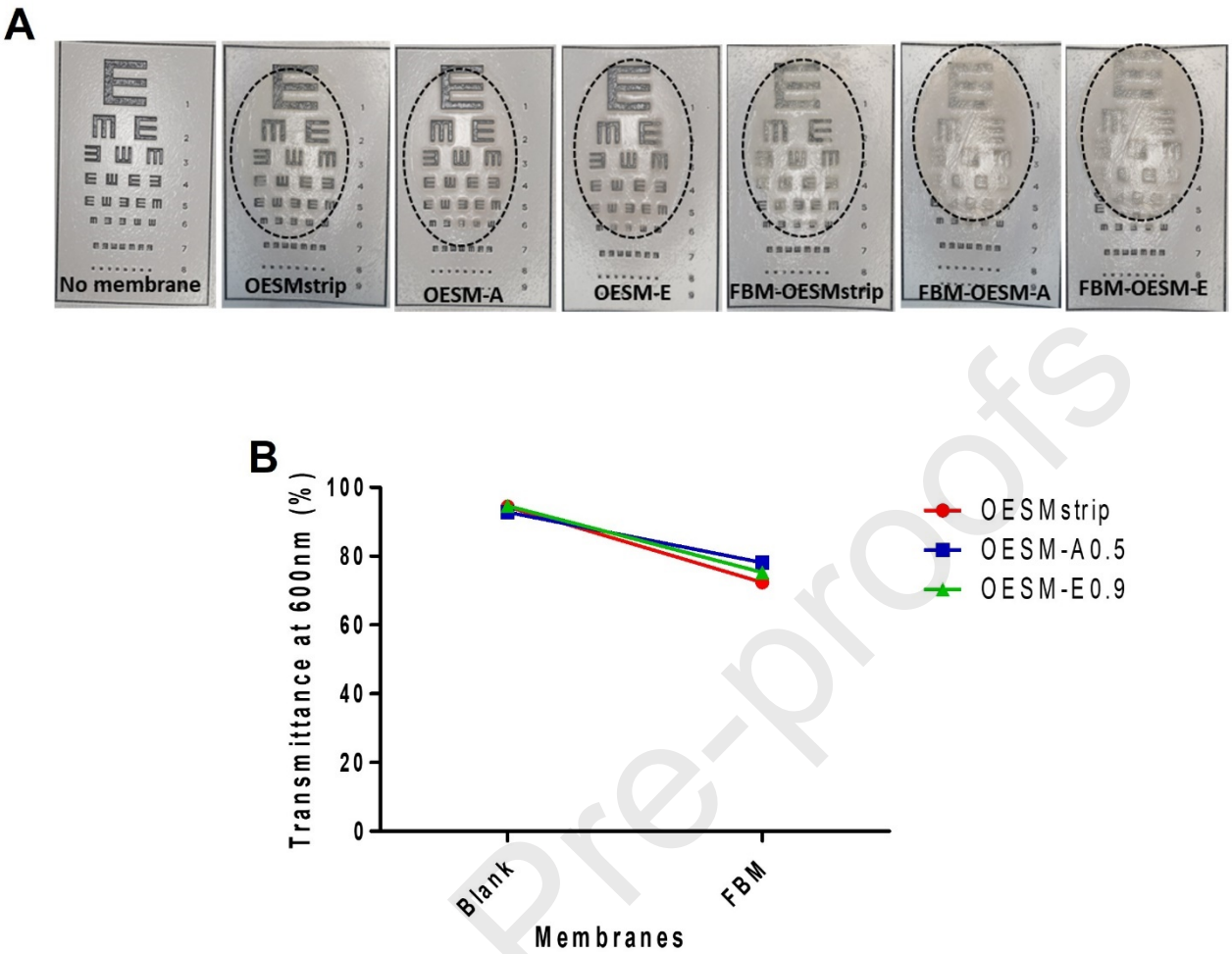

Figure 6. Transparency results. (A) Images representing the visual transparency of the outer and inner sides of the ESM samples (B) UV light transmittance profiles of membranes (Blank OESMstrip, Blank OESM-A, Blank OESM-E, FBM-OESMstrip, FBM-OESM-A and FBM-OESM-E) O: outer side membrane; FBM: FITC-BSA incorporated MP. All values are expressed as mean ± σ for n=6. 1 way ANOVA with Tukey's Multiple Comparison Test ($p<0.05$).

3.5 .Porosity

The fluid handling property of the drug incorporated MPs was assessed by measuring the porosity (Figure 7). The average porosity of the FITC-BSA incorporated MPs-ESM samples are significantly reduced as compared to the Blank OESM samples ($p < 0.001$). Comparing the porosity of the drug incorporated MPs-ESM produced, the FBM-OESMstrip is significantly lower than the FBM-OESM-A

and FBM-OESM-E ($p < 0.01$). In the case of FBM-OESM-A and FBM-OESM-E, no significant difference was observed ($P > 0.05$).

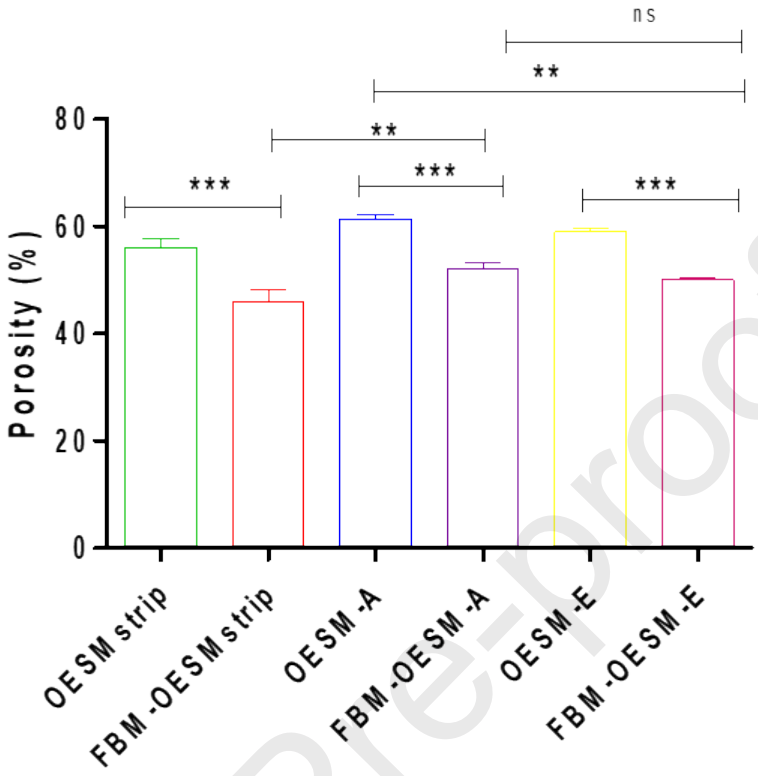

Figure 7. Porosity measurements drug incorporated MP-ESM. The liquid displacement method was employed in measuring the porosity of the Blank OESMstrip, Blank OESM-A, Blank OESM-E, FBM-OESMstrip, FBM-OESM-A and FBM-OESM-E. (*) which represents a $p < 0.05$, (**) which represents a $p < 0.01$, and (***) which represents a $p < 0.001$. No statistical significance (ns) is indicated by $p > 0.05$. All values are expressed as mean ± σ for n=3. 1-way ANOVA with Bonferroni's multiple comparison post-test ($p > 0.05$). FBM: FITC-BSA incorporated microparticles.

3.6. Wettability test

The contacts angles of the blank and drug incorporated MPs ESMs were assessed to study the wettability property of the bandage (Figure 8A). The contact angles of the blank ESMs are significantly lower than that of the FITC-BSA incorporated MPS-ESMs i.e., Blank OESMstrip vs FBM-OESMstrip, $p < 0.01$, Blank OESM-A vs FBM-OESM-A, $p < 0.05$ and Blank OESM-E vs FBM-OESM-E, $p < 0.01$. Additionally, no significant difference was observed the porosities of FBM-OESMstrip, FBM-OESM-A and FBM-OESM-E ($p > 0.05$).

3.7. Drug release study

The i*n vitro* % cumulative drug release profile fabricated membranes and Free PLGA (MPs were studied using a novel *in vitro* Franz cell model with porcine vitreous (Figure 8B). A higher percentage

of FITC-BSA release was found in the control i.e., FITC-BSA incorporated MPs compared with the release from the MPs incorporated ESM i.e., FBM-OESMstrip, FBM-OESM-A and FBM-OESM-E0. From the results, FBM-OESMstrip and FBM-OESM-A provided the maximum release of the FITC-BSA ($p>0.05$) followed by FBM-OESM-E. The MPs-ESMs showed a good, sustained release behaviour. The release of the drug from the ESMs was prolonged up to 10 days whereas in the case of the control > 50% was release within 7 days.

3.8. In ovo chorioallantoic membrane test

The angiogenic responses and biocompatibility of the drug incorporated ESMs were suing using CAM assay. The results of the samples: no treatment, PBS, VEGF, VEGF incorporated MPS, Blank MPs-OESMstrip, blank MPs-OESM-A, blank MPs-OESM-E, VM-OESMstrip, VM-OESM-A and VM-OESM-E are presented in Figure 8C. On the 10th day, the samples were imaged, and the number of branching vessels were counted using AngioQaunt software). From the results, (Figure 8C), the VEGF sample was provided as the control group (48.33 ± 17.89, $p<0.001$). All samples produced insignificant mean branch vessel counts ($p>0.05$) when compared to the control (no treatment, except VEGF ($p<0.001$), VEGF incorporated MPS ($p<0.05$) and VM-OESM-A ($p<0.05$). In considering the mean branch vessels counts of VEGF vs the VEGF incorporated MPs samples, no significant difference was observed in VEGF vs VEGF incorporated MPs, VM-OESMstrip, VM-OESM-A and VM-OESM-E ($p>0.05$). Similarly, insignificant branch vessels count was obtained for VEGF incorporated MPs vs VM-OESMstrip, VM-OESM-A and VM-OESM-E ($p>0.05$). In regard to the blank ESMs and their respective VEGF incorporated MPs ESMs, the mean branch vessels count was significant in OESMstrip/VM-OESMstrip ($p<0.01$), OESM-A/ VM-OESM-A ($p<0.01$) whereas the count in OESM-E0/ VM-OESM-E was insignificantly different ($p>0.05$). This result shows that the VEGF released from the VM-OESM-A was significant enough to increase blood vessels formation.

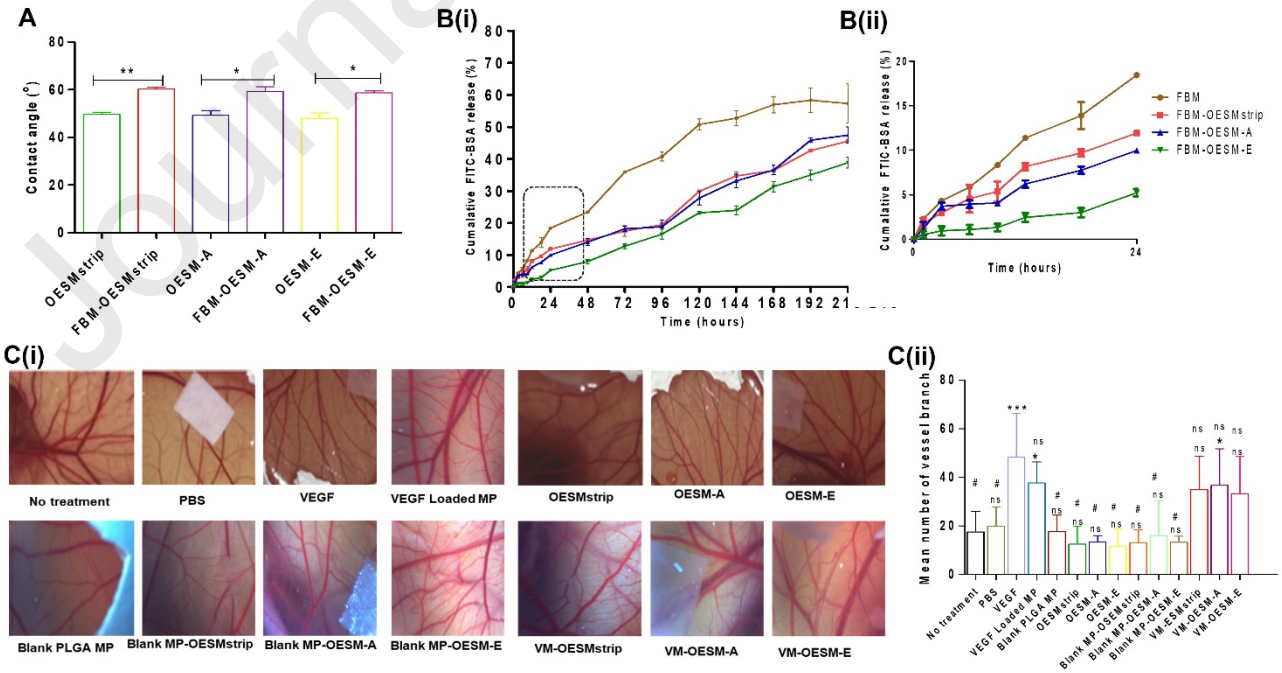

Figure 8. Additional characterization of the ESM (A) Wettability test. The contact angle of the blank and MP incorporated ESM was measuring the sessile drop method. At 10 seconds, the contact angle of the PBS droplet on the samples were measured using CAM 200 optical contact angle meter (KSV Instruments Ltd, Finland) at room temperature (19 °C). (*) which represents a $p < 0.05$, (**) which represents a $p < 0.01$, and (***) which represents a $p < 0.001$. No statistical significance (ns) is indicated by $p > 0.05$. All values are expressed as mean ± σ for n=3. 1-way ANOVA with Bonferroni's multiple comparison post-test ($p>0.05$). FBM: FITC-BSA incorporated microparticles (B) The % cumulative release of FITC-BSA release of FITC-BSA incorporated microparticles (control) and MP ESMs. Inert % cumulative release for the first 24 hours. All values are expressed as mean ± σ for n=3. FBM: FITC-BSA incorporated microparticles (C). Angiogenic profile analyses with (i) images summarizing the CAM assay, following 10 days of incubation at 37°C, and the presence of extracted ESM samples and controls. (ii) histogram indicating the number of blood vessel branches measured using AngioQaunt software expressed as mean ± σ. * corresponds to $p<0.05$; *** corresponds to $p<0.001$; ns: no significant difference (1-way ANOVA with Bonferroni's multiple comparison post-test; $p>0.05$ for no treatment as control). # corresponds to $p< 0.001$ (1-way ANOVA with Bonferroni's multiple comparison post-test; $p>0.05$ for VEGF as control). VEGF: vascular endothelial growth factor FBM: FITC-BSA incorporated microparticles VM: VEGF incorporated microparticle.

4. DISCUSSION

The treatment for chronic wound healing normally calls for the combination of bandages and concurrent application of topical drugs. Adherence to regular admiration of topic drugs is a major issue, henceforth there is a need to develop a 2-in-1 ocular bandage for convenient and cost-effective strategy for skin/ocular chronic wound healing. A drug incorporated bandage is useful in the treatment of chronic wounds. Its main indications are to relieve the pain, protect the ocular surface, promote corneal healing and epithelial regeneration and deliver ophthalmic drugs on the ocular surface (1, 49-52). It is crucial to consider these physical and surface properties such as thickness, transparency, modulus, wettability, water content, oxygen permeability and maximise drug loading capacity when developing the bandage (50). In this study a MPs were incorporated into ESM to produce cheap, effective and rapid wound bandage for patients. The generated bandage was characterised by evaluating the physical, mechanical and the biological properties.

Chemical modification is a simple technique through surface hydrolysis with an alkali or aminolysis. This method introduces hydrophilic carboxylic acids (-COOH) and hydroxyl (-OH) or amine groups through the cleavage of ester bonds which can be used to bind bioactive molecules such as collagen and chitosan (53-56). In order to modify the surface of the PLGA MPs, partial alkaline hydrolysis using 0.2 M NaOH was employed. The modified MPs were washed after the treatment to remove any NaOH residue. The modified MPs were successfully incorporated into the ESMs by using a spatula. The generated ESMs were washed, freeze dried and stored. The outer layer samples of OESMstrip, OESM-A, OESM-E, FBM-OESMstrip, FBM-OESM-A and FBM-OESM-E contained more than 60% MPs (Table 1). The highly interconnected, porous and large surface area of the outer side of ESM allows the inner

shell membrane of the ESMstrip, and outer shell membrane of the ESM-A and ESM-E act as an adsorbent of MPs (23, 35, and 57). The major component of the chicken ESM is collagen protein and Nakano, Ikawa and Ozimek (33) pointed out that the main chemical composition is amino acids. Thereby, lots of the amino functional groups on the ESMs are available to interact with free –COOH and –OH groups on the PLGA MPs surface.

FITC-BSA incorporated MPs with mean particle sizes of 17.09 ± 0.25 µm were incorporated into the outer side of ESMs and the structural morphology was analysed and compared with blank ESMs and FITC-BSA incorporated MPs. From the evaluations, the MPs were absorbed on the ESMs and verified by FESEM (Figure 3). The FESEM images demonstrated no difference in the fibrous structures of the blank OESMs (Figure 3A-C) and the MPs incorporated OESMs (Figure 3E-G). This observation was confirmed by measuring the fibre diameters of the FBM-OESMstrip, FBM-OESM-A and FBM-OESM-E and comparing them with the results of the fibre diameters of OESMstrip, OESM-A and OESM-E. Additionally, the MPs seen in the (FITC-BSA incorporated MPS: FBM-OESMstrip, FBM-OESM-A and FBM-OESM-E, Figure 3E-G respectively) have similar spherical shapes of varied sizes as the FITC-BSA incorporated MPs (FBM, Figure 3D). This establishes that the NaOH did not alter the morphology of the drug incorporated MPs.

The surface characteristics of the FITC-BSA MPs incorporated: ESMs: FBM-OESMstrip, FBM-OESM-A and FBM-OESM-E were further studies by measuring the surface roughness and compared to their respective blank ESMs: OESMstrip, OESM-A and OESM-E to understand their influence. It can be seen in Figure 4A-C that the blank ESMs appear rough, similar to the MPs incorporated ESMs (Figure 4D-F). The peaks or valleys on the sample's surface were determined by employing a microscopic quantitative technique. The mean arithmetical mean deviation, Ra for each ESM sample was deduced via Fiji-ImageJ software with SurfCharJ_Iq.class plugin by using FESEM images at magnification of 500x. The mean plot of FBM-OESMstrip, FBM-OESM-A and FBM-OESM-E and the Rs values produced for OESMstrip, OESM-A and OESM-E (Figure 4G) reveals that the surface changes by modifying the ESMs were statistically insignificant. This indicates that the incorporation of FITC-BSA MPs into the ESMs had no impact on the surface roughness.

The chemical composition of the FITC-BSA MPs incorporated ESM was evaluated by deploying Fourier transform infrared (FTIR) spectroscopy. The FTIR study was implemented to study interaction between the MPs and the ESM. Figure 5 shows the FTIR spectra of Blank ESM (natural), blank PLGA MPs, FBM-OESMstrip, FBM-OESM-A and FBM-OESM-E. From the data, the footprint of the natural ESM (i.e., 1646 cm^{-1}, 1524 cm^{-1}, 1441 cm^{-1} and 1240 cm^{-1}) and PLGA (i.e., 2946.72 - 3000 cm^{-1} and 1746.53 cm^{-1}) are identified in the FTIR spectra of the FBM-OESMstrip, FBM-OESM-A and FBM-OESM-E. The reduction of the -OH peak may be due to the interaction of the amino group in the ESM and the ester group in the MPs. This suggests that the FITC-BSA MPs were successfully immobilised on the surface of the OESMstrip, OESM-A and OESM-E.

One of the prominent characteristics of the cornea is its transparency, which is an important criteria consideration when selecting a material for cornea wound healing (23, 57-59). The transparency of wet blank ESMs and drug incorporated MPs ESMs was analysed using waterproof test card method (Figure 6A). The samples were placed on the card to determine the visibility of the test through the samples. The tests are obviously visible in all the samples however, the visibility in the FBM-OESMstrip, FBM-OESM-A and FBM-OESM-E is reduced as compared to the OESMstrip, OESM-A and OESM-E. The reduction was due to the presence of drug-incorporated MPs. Using UV-VIS spectrophotometer, the visibility of the samples was characterised by measuring the light transmittance. All the samples recorded light transmittance values above 80% (Figure 6B), however

the values of the MPs incorporated samples are below their corresponding neat ESMs. The reduction may be ascribed to the presence of the MPs.

Some of the main features of biomaterial for cornea wound healing applications such as wettability are related to the porosity (60). In this chapter, the fluid handling property of the drug incorporated MPs ESMs was evaluated by determining the porosity. The results (Figure 7) reveal that the porosity of the FBM-OESMstrip, FBM-OESM-A and FBM-OESM-E were significantly reduced as compared to their corresponding blank samples: OESMstrip, OESM-A and OESM-E. The decrease in porosity was due to the reduction of the pore size/volume in the bank ESMs samples by the incorporation of the FITC-BSA MPs.

Wettability (hydrophilicity and hydrophobicity) of bandages for cornea wound healing plays a role in the interaction of the bandages and the cornea tissues (60-61). In this study, the wettable behaviour of the FITC-BSA incorporated MPs ESM samples was evaluated by determining the contact angle. The data (Figure 8A) revealed that the contact angles of the FBM-OESMstrip, FBM-OESM-A and FBM-OESM-E increased significantly as compared to their respective blank samples OESMstrip, OESM-A and OESM-E. This observation shows that the surfaces of FITC-BSA incorporated MPs ESMs have lower hydrophilicity than the blank ESMs. According to Hsieh *et al*, (62), the contact angle measurement can be used to examine the surface roughness of materials. From this investigation, the modification of the ESMs by incorporating the FITC-BSA MPS increased the roughness of the samples. Intriguingly, the qualitative measurement of the surface roughness (Figure 8) contracts this observation as the roughness of the samples after the incorporation of MPs did not significantly alter the surface roughness.

The application of ESM as a drug delivery reservoir was examined in this study. The release profile of the model drug, FITC-BSA encapsulated in the MPs through ESMs were analysed using a novel *in vitro* France cell eye model constructed with a middle chamber containing porcine vitreous to stimulate the *in vivo* conditions of the eye (44). The FBM-OESMstrip, FBM-OESM-A and FBM-OESM-E achieved sustained drug release in vitro up to 10 days (Figure 8B). Sustained drug delivery directly into the corneal could circumvent patient compliance issues, the typical short residence time of ophthalmic drugs on the ocular surface, and the low efficacy of topical drugs (63-65).

The bioactivity/biocompatibility of the drug incorporated MPs ESMs was examined via the chorioallantoic membrane (CAM) assay. The CAM assay was carried out to determine the angiogenic profile of the MPs ESMS. Subsequently, vascular endothelial growth factor (VEGF) incorporated MPs were incorporated into the ESMs samples. VEGF is a key regular of blood vessel formation hence it has been utilized in several studies for the understanding of the angiogenic activity of biomaterials in the CAM assay (23, 66-68). The free VEGF, VEGF incorporated MPs (VM incorporated MPs), blank PLGA MPs, ESMs with and without VEGF incorporated MPs or blank PLGA MPs were incorporated on the CAM and examined on day 10 (Figure 8C). The quantitative analysis of the new blood vessel branches formation presented in Figure 8C(ii) shows that the blank PLGA MPs and ESM with or without the blank PLGA MPs did not significantly increase the formation of new blood vessel branches when contrasted with the control (no treatment, $p>0.05$). This observation is in a concurrence with a study by Zhao *et al*, 2009 (68), which demonstrated that PLGA MPs on CAM produce normal formation of blood vessels. Furthermore, the results attained for the blank ESMs samples validate the angiogenic profile of ESMs on CAM in Mensah *et al*, 2021 (23). Moreover, the VEGF incorporated samples on the CAM: the VEGF (positive control), $p<0.001$, VEGF incorporated MPs, $p<0.05$ and VM-OESM-A, $p<0.05$ had higher new blood vessel branches formation as compared to the control. This shows that the VEGF was successfully incorporated into the MPs and retained functionality. The

release of VEGF from VM-OESMstrip and VM-OESM-E was not adequate to cause a significant increase in blood vessel formation ($p>0.05$). With regards to a biomaterial for corneal wound healing, minimal vascularization is beneficial: the cornea is a transparent avascular tissue that accounts for excessive blood vessels formation will distort the clearness of the ocular surface.

5. CONCLUSION

In this study, intact and complete eggshell membranes (ESM) were successfully obtained using the in house optimised acetic and EDTA extraction methods. FITC-BSA incorporated PLGA MPs were fabricated and successfully deposited onto the outer layer of ESMs by a convenient surface adsorption and attachment technique. The 2 in 1 bandage consisting of the ESM and drug incorporated MPs was characterised accordingly. The incorporated MP was verified via FESEM and FTIR. The attachment process did not affect the morphology, fibre diameter, roughness and release profile of the FITC-BSA. Again, the presence of the incorporated MPs did not compromise the transparency of the bandage. The bandage exhibited a good biocompatibility property and did not promote pro-angiogenesis. Although the bandage exhibited promising cornea wound healing properties, *in vivo* wound healing will need to be undertaken to validate its effectiveness.

Declaration of conflicting interests: The author(s) declared no potential conflicts of interest with respect to the research, authorship, and/or publication of this article.

Funding: This work was supported by grants the Rosetrees Trust [Seedcorn Award] and the Stoneygate Trust.

Author contribution: RAM: Data curation, Formal analysis, Investigation, Methodology, Writing—original draft; **MTC:** Investigation, Methodology, Resources, Supervision, Writing—review and editing; **SBK:** Investigation, Methodology, Resources, Supervision, Writing—review and editing; **VH:** Investigation, Methodology, Resources, Supervision, Writing—review and editing; **DYSC**: Conceptualization, Data curation, Funding acquisition, Investigation, Methodology, Project administration, Resources, Supervision, Writing—review and editing. All authors have read and agreed to the published version of the manuscript.

6. REFERENCES

1. Bukowiecki A, Hos D, Cursiefen C, Eming SA. Wound-Healing Studies in Cornea and Skin: Parallels, Differences and Opportunities. Int J Mol Sci. 2017;18(6):1257. doi: 10.3390/ijms18061257. PMID: 28604651; PMCID: PMC5486079.
2. Sklenárová R, Akla N, Latorre MJ, Ulrichová J, Franková J. Collagen as a Biomaterial for Skin and Corneal Wound Healing. J Funct Biomater. 2022;13(4):249. doi: 10.3390/jfb13040249.
3. Hodge JG, Zamierowski DS, Robinson JL, *et al*. Evaluating polymeric biomaterials to improve next generation wound dressing design. Biomater Res. 2022;26(1):50. doi: 10.1186/s40824-022-00291-5.
4. Patel A. Ocular drug delivery systems: An overview. World J Pharmacol. 2013;2(2):47. doi: 10.5497/wjp.v2.i2.47.
5. Weng Y, Liu J, Jin S, Guo W, Liang X, Hu Z. Nanotechnology-based strategies for treatment of ocular disease. Acta Pharm Sin B. 2017;7(3):281-291. doi: 10.1016/j.apsb.2017.01.005.
6. Mensah RA, Kirton SB, Cook MT, Styliari ID, Hutter V, Chau DYS. Optimising poly(lactic-co-glycolic acid) microparticle fabrication using a Taguchi orthogonal array design-of-experiment approach. PLoS One. 2019;14(9):e0222858. doi: 10.1371/journal.pone.0222858. PMID: 31557205; PMCID: PMC6762136.
7. Korhonen E, Rönkkö S, Hillebrand S, *et al*. Cytotoxicity assessment of porous silicon microparticles for ocular drug delivery. Eur J Pharm Biopharm. 2016;100:1-8. doi: 10.1016/j.ejpb.2016.01.013.
8. Kothuri MK, Sahu S, Sahoo SK. Microparticles and nanoparticles in ocular drug delivery. In: Mitra AK, Cholkar K, Mandal A, eds. Ophthalmic Drug Delivery Systems. Routledge; 2021:437-466.
9. Dhyani A, Kumar G. A new vision to eye: Novel ocular drug delivery system. Pharmacophore. 2019;10(1):13-20.
10. Ljubimov AV, Saghizadeh M. Progress in corneal wound healing. Prog Retin Eye Res. 2015;49:17-45. doi: 10.1016/j.preteyeres.2015.06.001.
11. Nour S, Baheiraei N, Imani R, Khodaei M, Alizadeh A, Rabiee N, Moazzeni SM. A review of accelerated wound healing approaches: Biomaterial-assisted tissue remodeling. J Mater Sci Mater Med. 2019;30(12):120. doi: 10.1007/s10856-019-6348-5.
12. Holland G, Pandit A, Sánchez-Abella L, Haiek A, Loinaz I, Dupin D, Gonzalez M, Larra E, Bidaguren A, Lagali N, Moloney E, Ritter T. Artificial Cornea: Past, Current, and Future Directions. Front Med. 2021;8:770780. doi: 10.3389/fmed.2021.770780.
13. Bonnans C, Chou J, Werb Z. Remodelling the extracellular matrix in development and disease. Nat Rev Mol Cell Biol. 2014 Dec;15(12):786-801. doi: 10.1038/nrm3904.
14. Wilson SE. Corneal wound healing. Exp Eye Res. 2020;197:108089.
15. Kamil S, Mohan RR. Corneal stromal wound healing: Major regulators and therapeutic targets. Ocul Surf. 2021;19:290-306.
16. Deng X, Gould M, Ali MA. A review of current advancements for wound healing: Biomaterial applications and medical devices. J Biomed Mater Res B Appl Biomater. 2022 Nov;110(11):2542-2573. doi: 10.1002/jbm.b.35086.
17. Wang F., Wang M., She Z., Fan K., Xu C., Chu B., Chen C., Shi S., Tan R. Collagen/chitosan based two-compartment and bi-functional dermal scaffolds for skin regeneration. Mater. Sci. Eng. C. 2015;52:155–162. doi: 10.1016/j.msec.2015.03.013.

18. Ramshaw J.A.M., Werkmeister J.A., Glattauer V. Collagen-based Biomaterials. Biotechnol. Genet. Eng. Rev. 1996;13:335–382. doi: 10.1080/02648725.1996.10647934.
19. Williams C. Algosteril calcium alginate dressing for moderate/high exudate. Br. J. Nurs. 1999;8:313–317. doi: 10.12968/bjon.1999.8.5.6680.
20. Dhivya S., Padma V.V., Santhini E. Wound dressings—A review. BioMedicine. 2015;5:22. doi: 10.7603/s40681-015-0022-9.
21. Li E, Donati S, Lindsley K, Krzystolik M, Virgili G. Treatment regimens for administration of anti-vascular endothelial growth factor agents for neovascular age-related macular degeneration. Cochrane Database Syst Rev. 2020;10:CD011333.
22. Li F, Carlsson D, Lohmann C, Suuronen E, Vascotto S, Kobuch K, Sheardown H, Munger R, Nakamura M, Griffith M. Cellular and nerve regeneration within a biosynthetic extracellular matrix for corneal transplantation. Am J Ophthalmol. 2004;138(2):318.
23. Mensah RA, Jo SB, Kim H, Park SM, Patel KD, Cho KJ, Cook MT, Kirton SB, Hutter V, Sidney LE, Alves-Lima D, Lin H, Lee JH, Kim HW, Chau DY. The eggshell membrane: A potential biomaterial for corneal wound healing. J Biomater Appl. 2022;36(5):912-929. doi: 10.1177/08853282211024040. Epub 2021 Jun 18. PMID: 34139891; PMCID: PMC8606947.
24. Mensah RA, Salim K, Peszko K, Diop S, Wong TH, Chau DY. The chicken eggshell membrane: a versatile, sustainable, biological material for translational biomedical applications. Biomedical Materials. 2023 May 5
25. Briggs E, Mensah RA, Patel KD, Mandakhbayar NE, Sharifulden NS, Erdogan ZK, Barrios Silva LV, *et al*. Therapeutic application of an Ag-nanoparticle-PNIPAAm-modified eggshell membrane construct for dermal regeneration and reconstruction. Pharmaceutics. 2022;14(10):2162. doi: 10.3390/pharmaceutics14102162.
26. Ahmed T, Suso H, Maqbool A, *et al*. Processed eggshell membrane powder: bioinspiration for an innovative wound healing product. Mater Sci Eng C Mater Biol Appl. 2019;95:192-203. doi: 10.1016/j.msec.2018.10.021.
27. Baláž M. Eggshell membrane biomaterial as a platform for applications in materials science. Acta Biomater. 2014;10(9):3827-3843. doi: 10.1016/j.actbio.2014.05.005.
28. Chen X, Zhu L, Wen W, *et al*. Biomimetic mineralisation of eggshell membrane featuring natural nanofiber network structure for improving its osteogenic activity. Colloids Surf B Biointerf. 2019;179:299-308. doi: 10.1016/j.colsurfb.2019.03.036.
29. Shi Y, Zhou K, Li D, Guyonnet V, Hincke MT, Mine Y. Avian eggshell membrane as a novel biomaterial: a review. Foods. 2021;10(9):2178. doi: 10.3390/foods10092178.
30. Matsuoka R, Kurihara H, Yukawa H, *et al*. Eggshell membrane protein can be absorbed and utilised in the bodies of rats. BMC Res Notes. 2019;12(1):258. doi: 10.1186/s13104-019-4306-0.
31. Tsai WT, Yang JM, Lai CW, Cheng YH, Lin CC, Yeh CW. Characterization and adsorption properties of eggshells and eggshell membrane. Bioresource Technol. 2006;97(3):488-493. doi: 10.1016/j.biortech.2005.02.050.
32. Ruff KJ, DeVore DP, Leu MD, Robinson MA. Eggshell membrane: a possible new natural therapeutic for joint and connective tissue disorders. Results from two open-label human clinical studies. Clin Interv Aging. 2009;4:235-240. doi: 10.2147/cia.s5797.
33. Nakano T, Ikawa NI, Ozimek L. Chemical composition of chicken eggshell and shell membranes. Poult Sci. 2003;82(3):510-514. doi: 10.1093/ps/82.3.510.

34. Farjah G, Naeimi M, Saberi A. Comparison Outcome of Nerve Regeneration across an Eggshell Membrane Guidance Channel and Autograft. Caspian J Neurol Sci. 2016;2(4):1-8.
35. Choi HJ, Kim YM, Suh JY, Han JY. Beneficial effect on rapid skin wound healing through carboxylic acid-treated chicken eggshell membrane. Mater Sci Eng C Mater Biol Appl. 2021;128:112308. doi: 10.1016/j.msec.2021.112308.
36. Santana A, Melo A, Tavares T, Ferreira IMPLVO. Biological activities of peptide concentrates obtained from hydrolysed eggshell membrane byproduct by optimisation with response surface methodology. Food Funct. 2016;7(11):4597-4604. doi: 10.1039/C6FO00954A.
37. Sheish SG, Emadi R, Ahmadian M, Sadeghzade S, Tavangarian F. Fabrication and characterization of polyvinylpyrrolidone-eggshell membrane-reduced graphene oxide nanofibers for tissue engineering applications. Polymers. 2021;13(6):913. doi: 10.3390/polym13060913.
38. Sun P, Yan S, Zhang L, Zhang C, Wu H, Wei S, Xie B, Wang X, Bai H. Egg Shell Membrane as an Alternative Vascular Patch for Arterial Angioplasty. Front Bioeng Biotechnol. 2022;10:843590. doi: 10.3389/fbioe.2022.843590.
39. Wan QQ, Jiao K, Ma YX, *et al*. Smart, biomimetic periosteum created from the cerium(III, IV) oxide-mineralized eggshell membrane. ACS Appl Mater Interfaces. 2022;14(12):14103-14119. doi: 10.1021/acsami.2c01683.
40. Li X, Cai Z, Ahn D, Huang X. Development of an antibacterial nanobiomaterial for wound-care based on the absorption of AgNPs on the eggshell membrane. Colloids Surf B Biointerfaces. 2019;183:110449. doi: 10.1016/j.colsurfb.2019.110449.
41. Araújo C, Campos A, Padilha C, Júnior F, Alves do Nascimento R, Macedo G, Santos E. Enhancing enzymatic hydrolysis of coconut husk through Pseudomonas aeruginosa AP 029/GLVIIA rhamnolipid preparation. Bioresour Technol. 2017;237:10-16. doi: 10.1016/j.biortech.2017.03.178.
42. Amoyav B, Benny O. Microfluidic based fabrication and characterization of highly porous polymeric microspheres. Polymers (Basel). 2019;11(3):419. doi: 10.3390/polym11030419.
43. Chau D, Brown S, Mather M, *et al*. Tissue transglutaminase (TG-2) modified amniotic membrane: a novel scaffold for biomedical applications. Biomed Mater. 2012;7(4):045011. doi: 10.1088/1748-6041/7/4/045011.
44. Ahmed A, Boateng J. Calcium alginate-based antimicrobial film dressings for potential healing of infected foot ulcers. Ther Deliv. 2018;9(3):185-204. doi: 10.4155/tde-2017-0101.
45. Shafaie S, Hutter V, Brown M, *et al*. Influence of surface geometry on the culture of human cell lines: a comparative study using flat, round-bottom and V-shaped 96 well plates. PLoS One. 2017 Nov 3;12(11):e0186799. doi: 10.1371/journal.pone.0186799. PMID: 29099813; PMCID: PMC5667982.
46. Bible E, Qutachi O, Chau DY, Alexander MR, Shakesheff KM, Modo M. Neo-vascularization of the stroke cavity by implantation of human neural stem cells on VEGF-releasing PLGA microparticles. Biomaterials. 2012 Oct;33(30):7435-46. doi: 10.1016/j.biomaterials.2012.06.085. Epub 2012 Jul 18. PMID: 22818980; PMCID: PMC3418478.
47. Saif J, Schwarz TM, Chau DY, Henstock J, Sami P, Leicht SF, Hermann PC, Alcala S, Mulero F, Shakesheff KM, Heeschen C, Aicher A. Combination of injectable multiple

growth factor-releasing scaffolds and cell therapy as an advanced modality to enhance tissue neovascularization. Arterioscler Thromb Vasc Biol. 2010 Oct;30(10):1897-904. doi: 10.1161/ATVBAHA.110.207928. Epub 2010 Aug 5. PMID: 20689075.

48. Niemistö A, Dunmire V, Yli-Harja O, *et al*. Robust quantification of in vitro angiogenesis through image analysis. IEEE Trans Med Imaging. 2005 Apr;24(4):549-53. doi: 10.1109/TMI.2004.837339. PMID: 15822825.
49. Zidan G, Rupenthal I, Greene C, *et al*. Medicated ocular bandages and corneal health: potential excipients and active pharmaceutical ingredients. Pharm Dev Technol. 2018 Apr;23(3):255-260. doi: 10.1080/10837450.2017.1372195. Epub 2017 Sep 1. PMID: 28862034.
50. Son YJ, John WT, Zhou Y, Mao W, Yim EK, Yoo HS. Biomaterials and controlled release strategy for epithelial wound healing. Biomaterials Science. 2019;7(11):4444-4471. doi: 10.1039/C9BM00951E. PMID: 31549177.
51. Yu Y, Xu S, Li S, Pan H. Genipin-cross-linked hydrogels based on biomaterials for drug delivery: A review. Biomaterials Science. 2021;9(5):1583-1597. doi: 10.1039/d0bm01958h. PMID: 33543510.
52. Shah I, Jing L, Fei ZM, Yuan YS, Farooq MU, Kanjana N. A review on chemical modification by using sodium hydroxide (NaOH) to investigate the mechanical properties of sisal, coir and hemp fiber reinforced concrete composites. J Nat Fibers. 2022 Dec 1;19(13):5133-5151. doi: 10.1080/15440478.2022.2021969.
53. Pattison MA, Wurster S, Webster TJ, Haberstroh KM. Three-dimensional, nano-structured PLGA scaffolds for bladder tissue replacement applications. Biomaterials. 2005 May;26(15):2491-500. doi: 10.1016/j.biomaterials.2004.07.033. PMID: 15576125.
54. John AA, Subramanian AP, Vellayappan MV, Balaji A, Jaganathan SK, Mohandas H, Paramalinggam T, Supriyanto E, Yusof M. Physico-chemical modification as a versatile strategy for the biocompatibility enhancement of biomaterials. RSC Adv. 2015;5(49):39232-39244. doi: 10.1039/C5RA04271D.
55. Sadeghi AR, Nokhasteh S, Molavi AM, Khorsand-Ghayeni M, Naderi-Meshkin H, Mahdizadeh A. Surface modification of electrospun PLGA scaffold with collagen for bioengineered skin substitutes. Materials science and engineering: C. 2016 Sep 1;66:130-7.
56. Banerjee A, Panda S, Sidhantha M, *et al*. Utilisation of eggshell membrane as an adsorbent for carbon dioxide. International Journal of Global Warming. 2010;2:252. doi: 10.1504/IJGW.2010.032497.
57. Khosravimelal S, Mobaraki M, Eftekhari S, Ahearne M, Seifalian AM, Gholipourmalekabadi M. Hydrogels as emerging materials for cornea wound healing. Small. 2021 Jul;17(30):2006335. doi: 10.1002/smll.202006335.
58. Sklenářová R, Akla N, Latorre MJ, Ulrichová J, Franková J. Collagen as a Biomaterial for Skin and Corneal Wound Healing. Journal of Functional Biomaterials. 2022 Nov 16;13(4):249. doi: 10.3390/jfb13040249.
59. Chen Z, You J, Liu X, Cooper S, Hodge C, Sutton G, Crook JM, Wallace GG. Biomaterials for corneal bioengineering. Biomedical Materials. 2018 Mar 6;13(3):032002. doi: 10.1088/1748-605X/aaafcc.
60. Lampin M, Warocquier-Clérout R, Legris C, Degrange M, Sigot-Luizard MF. Correlation between substratum roughness and wettability, cell adhesion, and cell migration.

Journal of Biomedical Materials Research Part A. 1997 Jul;36(1):99-108. doi: 10.1002/(SICI)1097-4636(199707)36:1<99::AID-JBM14>3.0.CO;2-Q.

61. Salehi S, Fathi M, Javanmard SH, Bahners T, Gutmann JS, Ergün S, Steuhl KP, Fuchsluger TA. Generation of PGS/PCL blend nanofibrous scaffolds mimicking corneal stroma structure. Macromolecular Materials and Engineering. 2014 Apr;299(4):455-69. doi: 10.1002/mame.201300221.
62. Hsieh S, Chou H, Hsieh C, *et al*. Hydrogen peroxide treatment of eggshell membrane to control porosity. Food Chemistry. 2013;141:2117-2121. doi: 10.1016/j.foodchem.2013.05.012.
63. Tsai IL, Hsu CC, Hung KH, Chang CW, Cheng YH. Applications of biomaterials in corneal wound healing. J Chin Med Assoc. 2015 Apr 1;78(4):212-7.
64. Chau D, Tint N, Collighan R, Griffin M, Dua H, Shakesheff K, Rose F. The visualisation of vitreous using surface modified poly(lactic-co-glycolic acid) microparticles. Br J Ophthalmol. 2010 May;94(5):648-53.
65. Masli S, Sheibani N, Cursiefen C, Zieske J. Matricellular protein thrombospondins: influence on ocular angiogenesis, wound healing and immuneregulation. Curr Eye Res. 2014 Aug;39(8):759-74.
66. Schlingemann RO. Role of growth factors and the wound healing response in age-related macular degeneration. Graefes Arch Clin Exp Ophthalmol. 2004 Jan;242 Suppl 1:S91-101.
67. Rajappa M, Saxena P, Kaur J. Ocular angiogenesis: mechanisms and recent advances in therapy. Adv Clin Chem. 2010;50:103-21.
68. Zhao YH, Han LL, Chi YJ. Extracting hyaluronic acid from eggshell membrane with enzyme. Food Res Dev. 2008;1:40-3.

7. SUPPLEMENTARY MATERIAL

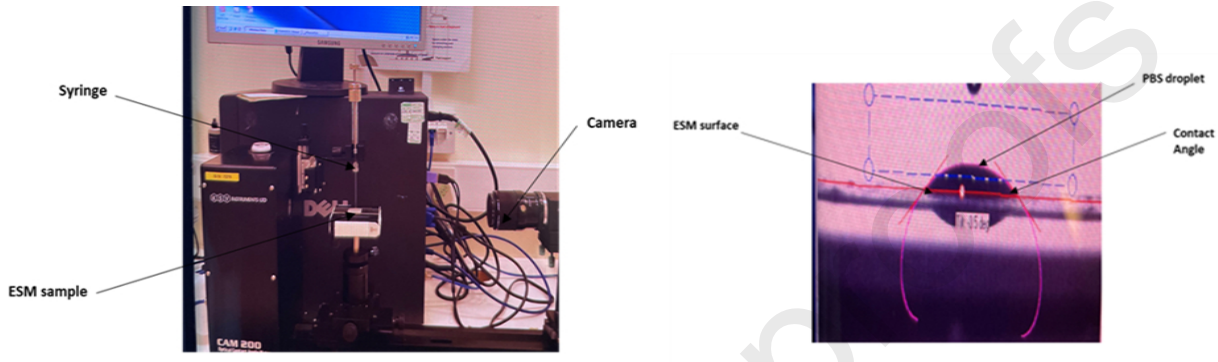

Figure S1: Photographs of wettability test using the sessile drop method. (a) KSV 200 CAM optical contact angle meter showing the mounted drug incorporated MP ESM sample. (b) Sessile drop measurement at room temperature (~19 °C).

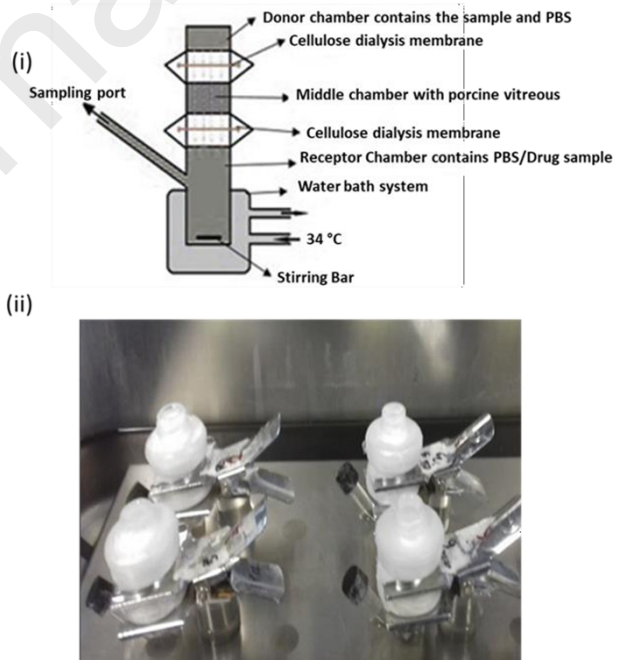

Figure S2. *In vitro* drug release study. (i) Schematic diagram of novel *in vitro* Franz diffusion cell eye model. FBM-OESMstrip, FBM-OESM-A or FBM-OESM-E mounted in the Franz cell eye model to evaluate the release s PBS: Phosphate buffer saline (ii) Photograph of Franz diffusion cells in water bath at 34°C. OESM represents outer layer of eggshell membrane and FBM represents Fluorescein isothiocyanate-labeled Bovine incorporated microparticles.

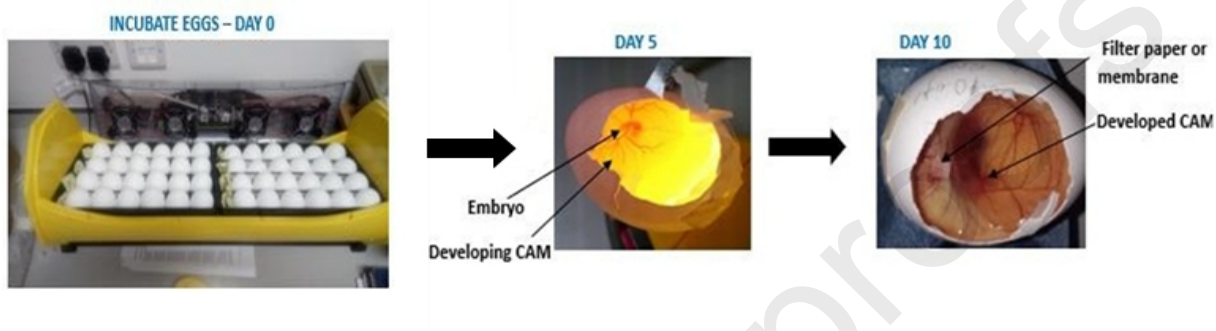

Figure S3. Angiogenic study. Fertilized eggs were incubated for 10 days to access the developed CAM in order to observe and compare the pro-angiogenic responses and release of the test samples introduced onto the CAM on day 5.